Synthesis and Characterization of $Ce_{0.9}Sm_{0.05}Pr_{0.05}O_{1.95}$ as a solid electrolyte for intermediate-temperature solid oxide fuel cell

Lemessa Asefa Eressa[1]*, PV Bhaskara Rao[2]

[1,2]Wollega University, Department of Physics, Nekemte, Ethiopia

Abstract : Co-doped sample of electrolyte$Ce_{0.9}Sm_{0.05}Pr_{0.05}O_{1.95}$have been preparedby Sol-gel method and characterized to explore its use as a solid electrolyte for intermediate temperature solid oxide fuel cells (IT-SOFCs).The crystal structure, microstructure, and ionic conductivity have been determined by X-ray diffraction (XRD), Scanning electron microscopy (SEM), Energy dispersive X-ray spectrometer (EDX), Raman Spectroscopy (Raman), and impedance spectroscopy, respectively. The XRD result reveals that the sample is single phase with cubic fluorite-type structure. The relative density of sample sintered at 1400^0C isabout98% of theoretical density. The average grain size of $Ce_{0.9}Sm_{0.05}Pr_{0.05}O_{1.95}$ sample found from SEM image is 451.4nm. The Raman spectra result showed formation of two distinctive peaks in the $Ce_{0.9}Sm_{0.05}Pr_{0.05}O_{1.95}$lattice. The peak at lower wavenumber (463) cm^{-1}) can be attributed to F_{2g} vibration mode (O-Ce-O) of the fluorite-like structure of pure CeO_2. Besides, the peak at higher wavenumber (564) cm^{-1} can be ascribed to the oxygen vacancies extrinsically introduced into $Ce_{0.9}Sm_{0.05}Pr_{0.05}O_{1.95}$ for maintaining the charge neutrality.The ionic conductivity and activation energy of $Ce_{0.9}Sm_{0.05}Pr_{0.05}O_{1.95}$found at 500^0C was(5.95 x10^{-3}S/cm, $Ea = 0.64eV$) respectively. All the results confirmed that $Ce_{0.9}Sm_{0.05}Pr_{0.05}O_{1.95}$is a promising alternative electrolyte for intermediate temperature solid oxide fuel cell (IT-SOFC) applications.

Key words : IT-SOFCS, electrolyte,$Ce_{0.9}Sm_{0.05}Pr_{0.05}O_{1.95}$, ionic conductivity.

1. Introduction

Solid oxide fuel cells (SOFCs) convert chemical energy directly into electrical energy with high efficiency and eco-friendly manner[1-9].However, in spite of these advantages, SOFC still has commercialization related problems such as its cost of fabrication at high temperature and durability [10-13]. One of the strategies which is supposed to be addressed to over come the bottle-neck of operating temperatures of SOFCs is finding an alternate solid electrolyte for intermediate temperature SOFCs (IT-SOFCs)[14-16].Ceria based oxides are explicitly being investigated for intermediate temperature applications due to their various advantages over ZrO_2 -based materials [17- 19].Among the various dopants of ceria studied, samaria doped

ceria (SDC) has received great attention as a potential IT-SOFC electrolyte due to its high ionic conductivity [20-24]. However, literature results indicated that the single-doped ceria based oxides have limitations for its application as solid electrolytes due to the tendency of reduction of Ce^{4+} (ionic conduction) to Ce^{3+} (electronic conduction)[25,26]. Furthermore, such low temperatures (500^0C-700^0C) are not still suitable for singly doped ceria as electrolyte in SOFC due to high grain resistance [27].

The author aimed on the preparation of co-doped ceria materials by Sol-Gel method in the $Ce_{0.9}Sm_{0.05}Pr_{0.05}O_{1.95}$material to investigate its structural and electrical properties for use as an electrolyte for IT-SOFC application.

2. Experimental

The sample with the general formula$Ce_{0.9}Sm_{0.05}Pr_{0.05}O_{1.95}$was synthesized through sol-gel method. High purity cerium(III) nitrate hexahydrate ($Ce(NO_3)_3.6H_2O$, 99.9%, Otto, India),Samarium(III) nitrate hexahydrate($Sm(NO_3)_3 .6H_2O$,99.9%, Otto, India) and Praseodymium(III) nitrate hexahydrate($Pr(NO_3)_3.6H_2O$, 99.9%, Otto, India) were used as the starting materials.

Stoichiometric amounts of all nitrates were dissolved in distilled water under continuous stirring. Citric acid was added to the whole mixture of precursors in 1:1 molar ratio to maintain the total molar ratio of metal to citric acid. In order to adjust the *p*H to ≈7, ammonium hydroxide was added drop by drop to the solution.

After adjusting pH value, the whole mixture was stirred at 80^0C for 2-3h and a homogenous solution was then formed. After 2-3h, a pale orange viscous gel was formed. The gel was placed in an oven to form ash. As the gel was put in an oven, slowly the gel started to foam, swell and finally burn with glowing flints and the evolution of large amounts of gas occurred. This auto ignition was slowly propagated until the whole sample was fully burnt to produce a light yellow colored ash. Ash was calcined at 700^oC for 2 h to remove the carbonaceous materials and the most stable mixed oxide phase was found. The resultant ash was ground continuously for 1h in agate mortar to get a fine homogeneous powder. The powders were pressed with the help ofa hydraulic press under a pressure of 200MPainto a circular pellet (8mm in diameter and 2 mm in thickness). Finally, the pellets were sintered in furnace at $1400^oC$for 2h and prepared for other measurement techniques.

The structural characterization of all the sintered sample was done at room temperature using Philips X-ray Diffractometer with Cuk$_\alpha$ radiation (λ=1.54 A^0) operated at 40 kV and 30 mA in the 2θ range of20–80° with a step size of 0.02 and a time for step is 2s. Experimental density was determined with Archimedes principle using xylene as a medium. Theoretical density was calculated from the molecular weight and uint cell volume (a^3). Relative density was calculated from the experimental density and theoretical density.

The morphology of sintered pellet wastaken by field- emission scanning electron microscope (FE-SEM, Carl Zeiss, Supra 40 VP).Ramanspectra of sintered pellets were recorded at room temperature with (a confocal WITec CRM 200, Germany, $\lambda = 532nm$).AC impedance measurements were carried out on pellets coated with silver paint on both surfaces employing Auto lab impedance Analyzer in the frequency range 1Hz-1MHzand in the temperature range of 300^0C-500^0C.

3. Results and Discussions

3.1 XRD Analysis

Fig. 1 shows the XRD patterns obtained from sample$Ce_{0.9}Sm_{0.05}Pr_{0.05}O_{1.95}$ sample that was prepared by sintering at 1400 ºC for 2 h. Eight symmetrical diffraction peaks were observed in the XRD spectra, and all samples can be indexed to single-phase cubic fluorite structure. It was found that the experimental lattice parameter of $Ce_{0.9}Sm_{0.05}Pr_{0.05}O_{1.95}$samplewasslightly larger than that of CeO_2 (5.411A^0), as expected from the effective ionic radii of Pr^{3+} and Sm^{3+}. Sine, the radii of Pr^{3+} (*r*= 1.126A^0) and Sm^{3+} (*r*= 1.08A^0) are greater than the radius of Ce^{4+} (*r*=0. 97A^0). Consequently, replacing Ce^{4+} with Pr^{3+} and Sm^{3+} cations in the lattice would lead to lattice expansion.

The experimental attice parameter 'a' can be calculated from the equation:

$$a = d.\sqrt{h^2 + k^2 + l^2} \qquad\qquad (1)$$

where, 'd' the inter planner distance and '*hkl*' are the Miller indices of the plane obtained in XRD measurement. Using Eq.1, the experimental lattice parameters of $Ce_{0.9}Sm_{0.05}Pr_{0.05}O_{1.95}$, calculated was 0.5447*nm* and depicted in Table1. This value is slightly larger than lattice parameter of pure CeO_2 (0.5411 *nm*) [28], as expected from the effective ionic radii of Pr^{3+} and Sm^{3+} (0.1103*nm*).

The crystallite size (D) is estimated using the Debye Scherrer's formula:

$$D = \frac{0.9\lambda}{\beta cos\theta} \qquad\qquad (2)$$

where, in the above equation (2), 'D' is the average particle size, 'β' is the full width at half maximum (FWHM) of X-ray reflection in terms of 2θ expressed in radians, 'θ' is the position of the diffraction peak in the diffract grams, λ is wave length of X-ray.

The average crystallite size of sample calculated using (Eq.2) was 14 nm. This result is consistent with the crystallite size found in previous literature[29]. It is clearly evident from the XRD pattern that only the peaks correspond to the ceria alone and that the absence of any other impurities was not reflected in the spectrum. Hence the single phase of $Ce_{0.9}Sm_{0.05}Pr_{0.05}O_{1.95}$ sample was used for further characterization techniques to test its electrical properties.
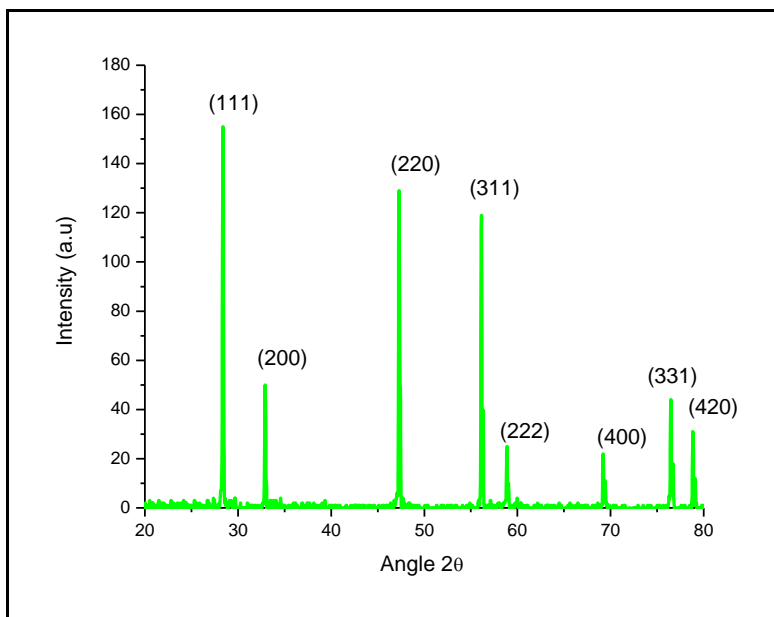
 Fig.1 XRD Patterns of $Ce_{0.9}Sm_{0.05}Pr_{0.05}O_{1.95}$ Sample

In this study, the density measurement was carried out to determine the extent of porosity in prepared sample. Theoretical density was calculated using the formula which is given as [30]:

$$D_t = \frac{4}{N_A a^3}[(1-x)M_A + xM_B + (2-0.5x)M_O] \qquad\qquad (3)$$

Where, '*x*' is the average mass of samarium and ytterbium content, '*a*' the lattice parameter at room temperature of samples, N_a the Avogadro number(6.023×10^{23}), M_A, M_B, and M_O refers atomic weights of cerium, average weights of samarium and praseodymium, oxygen respectively.

The relative density η is calculated as a relation in percentage of the sample density (D_e) to the theoretical density (D_t):

$$\eta = \frac{D_e}{D_t} x\ 100\% \qquad\qquad (4)$$

The theoretical, experimental and relative densities of $Ce_{0.9}Sm_{0.05}Pr_{0.05}O_{1.95}$ samplewere shown in Table 1. As it can be observed from Table1,the calculated relative density of $Ce_{0.9}Sm_{0.05}Pr_{0.05}O_{1.95}$ samplewas about 98% of the theoretical density and this finding was supported by SEM image.

Table 1. Grain size, lattice parameter and relative densities of Ce$_{0.9}$Sm$_{0.05}$Pr$_{0.05}$O$_{1.95}$sample.

Crystallite Size(nm)	14
Grain size (nm)	451.4
Grain size (nm)	5.447
Theoretical Density(g/cm^3)	7.22186
Experimental Density(g/cm3)	7.12768
Relative density	98.7

3.2. SEM and EDS Analysis

The surface morphology and chemical composition of Ce$_{0.9}$Sm$_{0.05}$Pr$_{0.05}$O$_{1.95}$, which were observed and analyzed by SEM and EDS are shown in Fig.2a and Fig.2b respectively.SEM micrograph clearly shows the presence of uniform grains with clean and distinct grain boundaries. As shown in Table 1, the average grain size of the material found from SEM graphs was 451.4(nm). As indicated in Fig 2b, the EDX graph reveals that all elements like Pr, Sm, Ce and O are entered in the lattice as per stochimetry and depicted in Table 2.

(a

(b
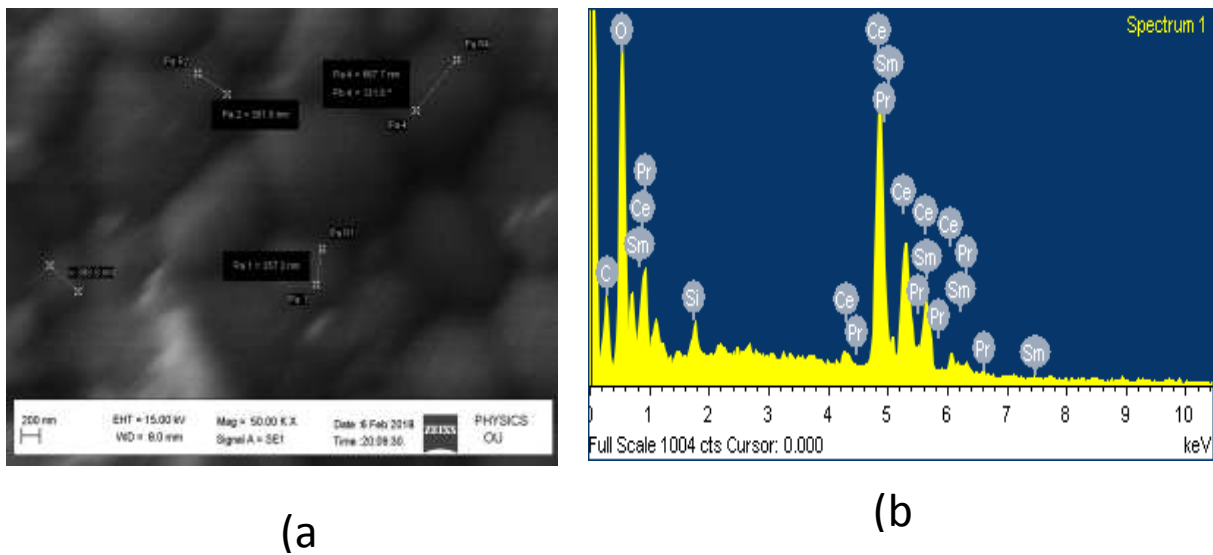
Fig.2 (a)SEM, (2b) EDX- graphs of Ce$_{0.9}$Sm$_{0.05}$Pr$_{0.05}$O$_{1.95}$

Table 2EDX quantitative analysis of elements O, Ce, Sm and Pr.

Element	Weight (%	Atomic(%)
O K	19.26	67.76
Ce L	67.90	27.87
Pr L	6.38	2.25
Sm L	6.46	2.12

3.3. Raman Spectroscopy

Fluorite structure-metal dioxides have only a single allowed Raman mode, which has F2g symmetry and can be viewed as a symmetric breathing mode of the oxygen(O) atoms around each cation. Since only the oxygen (O) atoms move, the mode frequency should be nearly independent of the cation mass. In CeO_2, this frequency is 465 cm^{-1}[31].

Raman spectra of the $Ce_{0.9}Sm_{0.05}Pr_{0.05}O_{1.95}$ sample, presented in Figure 4,show the presence of two characteristic peaks. The peak at lower wavenumber 463 (cm^{-1})can be attributed to F_{2g} vibration mode (O-Ce-O) of the fluorite-like structure of pure CeO_2. Besides, the peak at higher wavenumber (564) cm^{-1} can be ascribed to the oxygen vacancies extrinsically introduced into $Ce_{0.9}Sm_{0.05}Pr_{0.05}O_{1.95}$ for maintaining the charge neutrality. The changes in the Raman spectra are related to oxygen(O) vacancies introduced into the cation lattice (bivalent Pr^{3+} and Sm^{3+} is substituted for Ce^{+4}). This behavior of result was also found in previous literature [32-34]. Interestingly, with Pr doping, there is a slight, but systematic, shift of the F2g band to lower wavenumber accompanied by a decrease in the peak intensity compared with CeO_2.This is due to the larger ionic radius of Pr^{3+} (1.126 Å) relative to Ce^{4+} (0.97 Å), which, as seen from XRD analysis in an increase in the lattice parameter with increasing Pr doping. From the Raman spectroscopy, analysis, no indications can be found regarding the presence of impurities which is in good agreement with the XRD analysis depicted in (Fig.1).
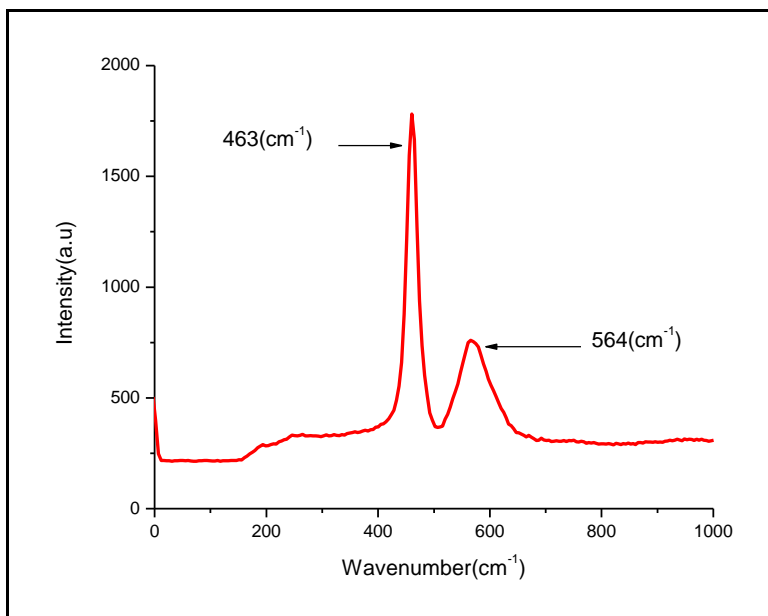
Figure3 Raman spectra of $Ce_{0.9}Sm_{0.05}Pr_{0.05}O_{1.95}$samplesintered at 1400^0C.

3.4. Impedance Spectroscopy

The complex impedance spectra for $Ce_{0.9}Sm_{0.05}Pr_{0.05}O_{1.95}$sample measured at 300^0C-500 ^{0}C in air are shown (Fig.4a –e). As illustrated in (Fig.4a-e), the intercept from starting point of high-frequency semicircle to real axis is the grain resistance Rg, the diameter of medium- frequency semicircle corresponds to the grain boundary resistance Rgb, the intercept of low-frequency end of medium-frequency semicircle to real axis is the total resistance $R=R$g+Rgb, the low-frequency curve can be attributed to the interface resistance Re between electrolyte and electrode.

The total resistance is given by-

$$R = R_g + R_{gb} \hspace{3cm} (5)$$

Where Rg and Rgb stand for the resistance of grain interior and grain boundary respectively.

The ionic conductivity (σ) of each sample was calculated using the equation:

$$\sigma = \frac{l}{RA} \qquad\qquad\qquad (6)$$

where l is the thickness of sample and Ais the cross-sectional area. Through fitting the data and using Eqs. (5) and(6), the ionic conductivity of sample at different temperatures was obtained. This result is presented in Table 3.

Table 3 Resistance and conductivity of $Ce_{0.9}Sm_{0.05}Pr_{0.05}O_{1.95}$ sample sintered at1400^{0}C .

Temperature(^{0}C)	$Rg(\Omega)$	$Rgb(\Omega$	$R_T(\Omega$	$\sigma(S/cm)$
300	260.85	2225.75	2486.16	2.87x10^{-4}
350	146.53	931.9	1078.43	6.62x10^{-4}
400	78.54	361.87	440.41	1.62x10^{-3}
450	52.4	168.38	220.8	3.23x10^{-3}
500	44.27	75.73	120.0	5.95x10^{-3}

As shown in Tables3, the conductivity of $Ce_{0.9}Sm_{0.05}Pr_{0.05}O_{1.95}$ sample increases with the rise of measuring temperature and a maximum conductivity of 5.95x10^{-3} (S/cm) was obtained at 500^{0}C. This is due thermal excitations which enhances the kinetic energy of carriers and force oxygen ions to pass through oxygen vacancies in a higher speed.
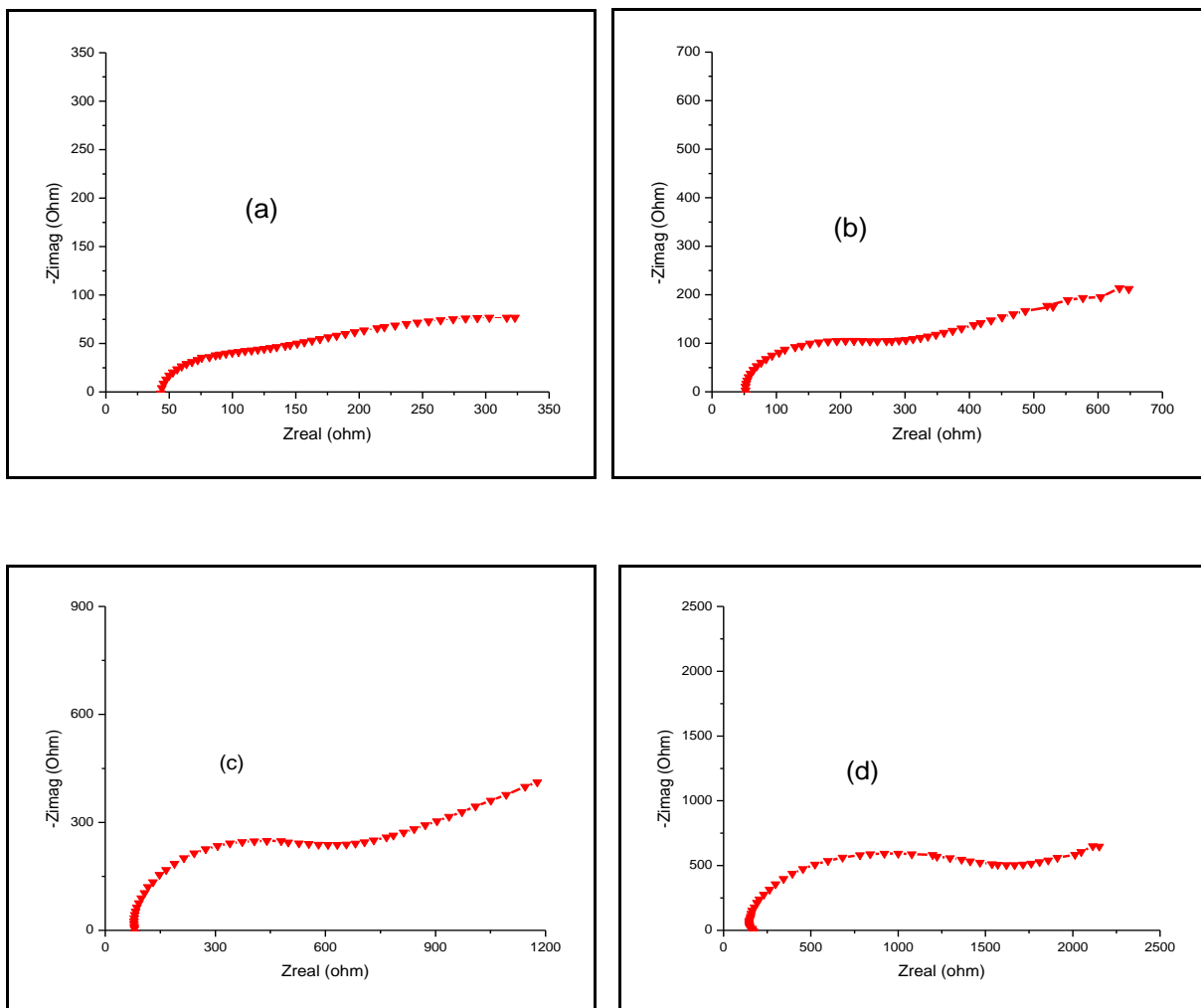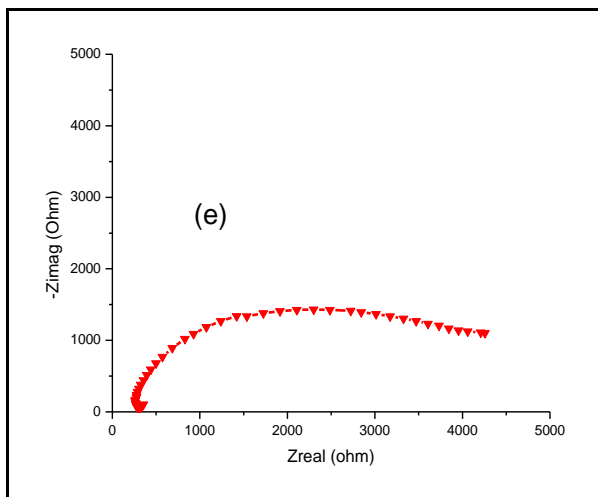
Figure 4Impedance plots of $Ce_{0.9}Sm_{0.05}Pr_{0.05}O_{1.95}$ sample measured in air at (a) 500 ^{0}C (b) 450ºC (c) 400 ^{0}C (d) 350 ^{0}C (e) 300 ^{0}C

The temperature dependence of ionic conductivity often follows an Arrhenius relation:

$$\sigma T = \sigma_o e^{-Ea/kT} \tag{7}$$

where Ea is the activation energy for conduction, T is the absolute temperature, k is the Boltzmann's constant and σ_o is a pre-exponential factor.The total ionic conductivity of $Ce_{0.9}Sm_{0.05}Pr_{0.05}O_{1.95}$ sample sintered at 1400^{0}C for 2h was presented in Fig.6 in the form of $\ln(\sigma T)$ versus $\left(10^3/T\right)$. The value of activation energy (Ea) of $Ce_{0.9}Sm_{0.05}Pr_{0.05}O_{1.95}$ sample calculated using (Eq.7) and slope fitting of (Fig.6) is 0.64eV.
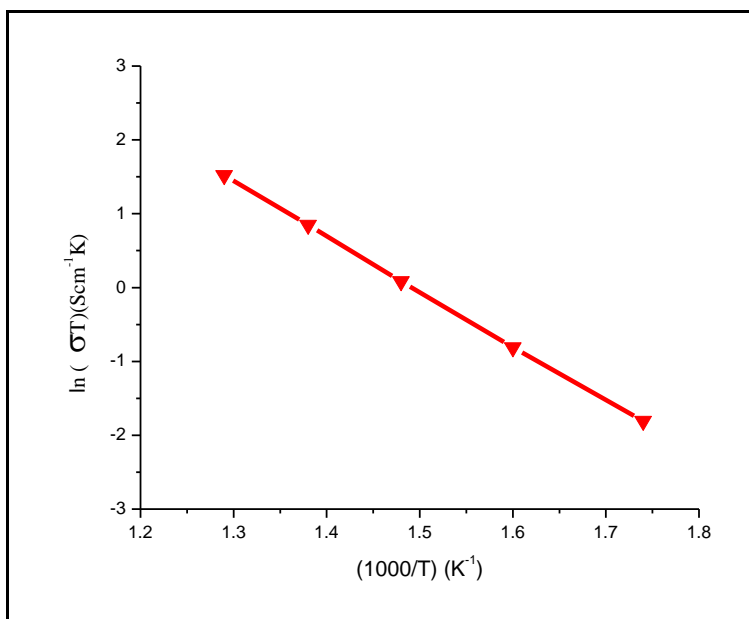
Figure.6 Arrhenius plots of total conductivity of $Ce_{0.9}Sm_{0.05}Pr_{0.05}O_{1.95}$sample.

4. Conclusion

$Ce_{0.9}Sm_{0.05}Pr_{0.05}O_{1.95}$ was successfully prepared through sol-gel method. The sample pellet was sintered at 1400^{0}C for 2h to obtain dense ceramic and the calculated relative density was about 98% of the theoretical density. The ionic conductivity and activation energy of $Ce_{0.9}Sm_{0.05}Pr_{0.05}O_{1.95}$ sample found at 500^{0}C was (5.95 x10^{-3}S/cm, Ea = 0.64eV) respectively. The ionic conductivity value obtained at such a lower operating temperature, 500^{0}C in this work was found to be higher than those of the values reported earlier in the

literature for singly doped ceria with praseodymium or samarium. Moreover, all the experimental results showed that the material prepared from $Ce_{0.9}Sm_{0.05}Pr_{0.05}O_{1.95}$ can be used as an electrolyte for intermediate temperature SOFC (IT-SOFCs) application.

5. References

1. I. Shajahana, J. Ahnb, P. Naira, S. Medisettia, S. Patila,V. Nivedithaa, G. U. B. Babuc, H. P.Dasaria, J.H. Leeb, Praseodymium doped ceria as electrolyte material for IT-SOFC applications, Mater. Chem. Phys. 2016(2018) 136-142.
2. Y. Gan, J. Cheng, M. Li, H. Zhan, W. Sun, Enhanced ceria based electrolytes by codoping samaria and Scandia for intermediate temperature solid oxide fuel cells,Mater. Chem. Phys. 163(2015) 279-285.
3. A. S. Kumar, R. Balaji, S. Jayakumar,C. Pradeep, Microwave assisted sintering of gadolinium doped barium cerate electrolyte for intermediate temperature solid oxide fuel cells,Mater. Chem. Phys. 182(2016) 520-525.
4. A. S. Kumar, R. Balaji, S. Jayakumar, Thermal, structural and electrical properties of samarium dopedbarium cerate electrolyte for SOFCs, Mater. Chem. Phys. 202(2017) 82-88.
5. S. Kobi, N. Jaiswal, D. Kumar, O. Parkash, Ionic conductivity of Nd^{3+} and Y^{3+} co-doped ceria solid electrolytes for intermediate temperature solid oxide fuel cells,*J. Allo. Comp.*(2015).
6. K. Venkataramana, C. Madhuri, Y. S. Reddy, G.Bhikshamaiah, C. V. Reddy, Structural, electrical and thermal expansion studies of tri-doped ceria electrolytematerials for IT-SOFCs, *J. Allo. Comp.* (2017).
7. C. E. Jeyanthi, R. Siddheswaran, P. Kumar, M. K. Chinnu, K. Rajarajan, R. Jayavel, Investigation on synthesis, structure, morphology, spectroscopic andelectrochemical studies of praseodymium-doped ceria nanoparticles by combustion method, Mater. Chem. Phys.151 (2015) 22-28.
8. G. Donmez, V. Sarıboga, T. G. Altıncekic , M. A. Faruk Oksuzomer, Polyol Synthesis and Investigation of $Ce_{1-x}RE_xO_{2-x/2}$ (RE = Sm, Gd, Nd, La,$0 \le x \le 0.25$) Electrolytes for IT-SOFCs, J.. Am. Ceram. Soc. (2014) 1–9.
9. Damisih, J. Raharjo, Masmui, R. S. Aninda, N. A. Lestari, Synthesis and Characterization of La, Sc, Yb and Nd codoped Gadolinium doped Cerium (GDC) Composite Electrolyte for IT-SOFC, Journal of Physics: Conf. Series 877 (2017) 012077.
10. M. Choolaeia, Q.Caia, Robert C.T. Sladeb, B. A. Horria, Nanocrystalline gadolinium-doped ceria (GDC) for SOFCs by an environmentally-friendly single step method, Ceram. Int. 44 (2018) 13286–13292.
11. S. Ramesh, K.C. J. Raju,Preparation and characterization of $Ce_{1-x}(Gd_{0.5}Pr_{0.5})_xO_2$electrolyte for IT-SOFCs, int. J. hydrogen energy 37(2012)10311-10317.
12. Z. Shao, W. Zhou, Z. Zhu, Advanced synthesis of materials forintermediate-temperature solid oxide fuel cells, Progress in Mat. Sci. 57 (2012) 804–874.
13. Y. Xia, X. Liu, Y. Bai, H. Li, X. Deng, X. Niu, X. Wu, D. Zhou, Z. Wang, J. Meng, Electrical properties optimization of calcium Co-dopingsystem: $CeO_2Sm_2O_3$, Int.J. hydrogen energy 37(2012)11934-11940.
14. J. Molenda, K. Swierczek, W. Zaj,Functional materials for the IT-SOFC,J. Power Sources 173 (2007) 657–670.
15. S. Omar, E. D. Wachsman, J. C. Nino,Higher ionic conductive ceria-based electrolytes for solid oxide fuel cells,Appl. Phys. Lett. 91, 144106 (2007); doi: 10.1063/1.2794725.
16. A. Tarancón, Strategies for Lowering Solid Oxide Fuel Cells Operating Temperature, *Energies 2(*2009)1130-1150; doi: 10.3390/en20401130.
17. G. Kim, N. Lee , K.B. Kim, B. K. Kim, H. Chang, S.J. Song, J.Y. Park,Various synthesis methods of aliovalent-doped ceria andtheir electrical properties for intermediate temperature solidoxide electrolytes, Int.J.Hydrogen energy 38(2013)1571-1587.
18. L. Spiridigliozzi, G. Dell'Agli, A. Marocco, G.Accardo,C. Ferone, R. Cioffi, Hydrothermal synthesis at low temperature gadolinium doped ceria,Proceedings of EFC2015.
19. G. Accardo, C. Ferone, R. Ciof, D.Fratni, L. Spiridigliozzi, G. Dell'Agli, Electrical and microstructural characterizaton ofceramic gadolinium-doped ceria electrolytes forITSOFCs by sol-gel route,J .Appl. Biomater. Funct.Mater.14(1)(2016) e35-e41,DOI: 10.5301/jabfm.5000265.
20. P. C. C. Dazaa, R. A. M. Menesesa, A. C. M. Rodrigues, C. R. M. Silvaa,Ionic conductivities and high resolution microscopic evaluation of grain andgrain boundaries of cerium-based codoped solid electrolytes, Ceram. Int. 44 (2018) 13699–13705.

21.   T. Karaca, T. G.Altıncekic¸M. Faruk. Oksuzomer, Synthesis of nanocrystalline samarium-doped CeO2 (SDC) powdersas a solid electrolyte by using a simple solvothermal route, Ceram. Int. 36 (2010) 1101–1107.

22.   M. R. Kosinski, R. T. Baker,Preparation and property–performance relationships in samarium-doped ceria nanopowders for solid oxide fuel cell electrolytes,J. Power Sources 196 (2011) 2498–2512.

23.   A. Arabaci, Effect of Sm and Gd dopants on structural characteristics and ionic conductivity of ceria,Ceram. Int.41 (2015) 5836–5842.

24.   G. Dell'Aglia, L. Spiridigliozzia, A. Maroccoa, G. Accardoc, D. Frattinid, Y. Kwond, S.P. Yoon, Morphological and crystalline evolution of Sm-(20 mol%)–doped cerianano powders prepared by a combined co-precipitation/hydrothermal synthesis for solid oxide fuel cell applications, Ceram. Int.43 (2017) 12799–12808.

25.   Y.Ch. Wu, C.C. Lin,The microstructures and property analysis of aliovalent cations (Sm^{3+}, Mg^{2+}, Ca^{2+}, Sr^{2+}, Ba^{2+})co-doped ceria-base electrolytes after an aging treatment, Int. J. hydrogen energy 39(2014)7988-8001.

26.   Sandhya K, Chitra Priya N. S., Aswathy P K, D. N Rajendran, impact of reduced sintering temperature on the grain size of samarium doped ceria electrolyte, Int.J.journal of Advance Research in Science and Engineering 6(2017).

27.   N. K. Singh, P. Singh, D. Kumar, O. Parkash, Electrical conductivity of undoped, singly doped, and co-doped ceria ,Ionics18 (2012) 127–134 ,DOI 10.1007/s11581-011-0604-9 .

28.   M.L. Dos Santos, R.C. Lima, C.S. Riccardi, R.L. Tranquilin, P.R. Bueno, J.A. Varela, E. Longo, Preparation and characterization of ceria nanospheres by microwave-hydrothermal method, Materials Letters 62 (2008) 4509–4511.

29.   Jeyanthi, C. E., et al. (2015). "Investigation on synthesis, structure, morphology, spectroscopic and electrochemical studies of praseodymium-doped ceria nanoparticles by combustion method." Materials Chemistry and Physics**151**: 22-28.

30.   J. Yang, B. Ji, J. Si, Q. Zhang, Q.Yin,J. Xie, C. Tian, Synthesis and properties of ceria based electrolyte for IT-SOFCs, Int. J. hydrogen energyy41(2016015979-15984.

31.   McBride, J., et al. (1994). "Raman and x-ray studies of Ce1− x RE x O2− y, where RE= La, Pr, Nd, Eu, Gd, and Tb." Journal of Applied Physics**76**(4): 2435-2441.

32.   Dohcevic-Mitrovic, Z., et al. (2007). "Temperature-dependent Raman study of Ce0. 75Nd0. 25O2-delta nanocrystals." Applied Physics Letters**91**(20).

33.   Ahn, K., et al. (2012). "Role of multivalent Pr in the formation and migration of oxygen vacancy in Pr-doped ceria: Experimental and first-principles investigations." Chemistry of Materials**24**(21): 4261-4267.

34.   Shajahan, I., et al. (2018). "Praseodymium doped ceria as electrolyte material for IT-SOFC applications." Materials Chemistry and Physics.

✶✶✶✶✶